Journal of Catalysis **183,** 24–31 (1999)
Article ID jcat.1998.2320, available online at http://www.idealibrary.com on IDEAL®

Structural Analysis of Au/TiO_2 Catalysts by Debye Function Analysis

D. A. H. Cunningham,*,[1] W. Vogel,† R. M. Torres Sanchez,‡ K. Tanaka,* and M. Haruta*

*Osaka National Research Institute, Midorigaoka 1, Ikeda City, Osaka 563-8577, Japan; †Fritz-Haber-Institut der Max-Planck-Gesellschaft, Faradayweg 4-6, D14195 Berlin (Dahlem), Germany; and ‡Mineral Resources and Ceramic Technological Center (Cetmic) Cno, Centenario y 506-CC49-(1897) M.B., Gonnet, Argentina

Received May 29, 1998; revised November 2, 1998; accepted November 2, 1998

Catalysts comprising between 1 and 3.6 wt% Au on TiO_2 have been studied by Debye function analysis. The structure of the deposited particles in Au/TiO_2, prepared by deposition–precipitation, in the presence of magnesium citrate, was predominantly fcc cuboctahedral, with a size distribution between 3 and 4 nm. Optimized fits indicate a twin probability of ~9%. Au/TiO_2 catalysts prepared by photodeposition were found to be much less active for CO oxidation than catalysts prepared by deposition–precipitation and comprised fcc cuboctahedral particles between 1 and 7 nm in size. © 1999 Academic Press

Key Words: **gold; TiO_2; catalysis; Debye function analysis; crystal structure; nanoparticles.**

1. INTRODUCTION

In recent years, because of the efforts of many groups, the catalytic activity of gold has become widely recognized. In general, most experimental results have shown that on large extended Au surfaces, oxygen is unable to adsorb on the (110) or (111) faces, and that over gold plates, molecular oxygen is chemically inert unless exposed to electric discharge (1), microwaves (2), or ozone (3). On relatively clean gold powders of submicrometer size, surface-adsorbed oxygen molecules become active, however, and the material shows high catalytic activity (4), even without the aid of electric discharge or microwave excitation. Not surprisingly several hypotheses have been put forth to explain the difference in activity, but beyond the observation that the activity of nanometer gold apparently derives from the ability of molecular oxygen to chemisorb onto the surface of the particle with Brønsted base character (5), the reason for the sudden chemical activity of gold remains largely a mystery.

One of the most plausible explanations for the high activity of nanometer gold put forward over the last 10 years emphasizes the structural aspects of the interface between gold and its support. However, as it is difficult to define with any accuracy the structure of the support, the importance of the interface is still at present unclear. Another explanation for the activity of gold has therefore become popular that it takes into account the different crystal structures exist at nanometer sizes. In essence, at small sizes (approaching the nanometer region) it is possible for Au crystals to take any one of several different structures. If the catalytic reaction is structure sensitive, it is then apparent that slight changes in the crystal symmetry may result in large chemical changes.

In attempts to confirm which of the two models is correct we have recently carried out initial experiments on a $Au/Mg(OH)_2$ catalyst (6, 7), that appear to indicate that the structure of the Au particle is the most important parameter in defining the catalytic activity. At small sizes, the most stable structures are the truncated octahedral series, the standard octahedral structures, and the catalytically active Mackay icosahedral species (6–15). In larger crystals, the face-centered cubic (fcc) cuboctahedral is the most stable structure (16–18). Unfortunately, in our previous work it was not possible to determine the surface structure of the support. Thus, even though the initial results are promising, the results we obtained still do not make it clear whether the change in catalytic activity associated with changes in crystal structure from fcc cuboctahedral to icosahedral is a general phenomenon (i.e., the icosahedral structure is required in all gold catalysts), or the structure and chemical behavior of each catalyst are unique and must be considered separately. This point is extremely important to resolve if theoretical studies are to become possible.

The system that we chose in an attempt to resolve this question was based on the Au/TiO_2 system. Au/TiO_2 is one of the most frequently studied systems due to the belief that TiO_2 is the best metal oxide for studying the so-called strong metal support interaction (SMSI). Also, the system is of interest as it is the only catalytic system to show the so-called "switching mechanism" through which the catalyst changes from an oxidative to a reductive catalyst simply through changes in Au particle size. Above 2 nm, Au/TiO_2 acts as a partial oxidative catalyst (which assists in the formation of propylene oxide from propylene), whereas below 2 nm, Au/TiO_2 causes the reduction of propylene to propane

[1] To whom correspondence should be addressed. Fax: (+81) 727-51-9631.

0021-9517/99 $30.00
Copyright © 1999 by Academic Press
All rights of reproduction in any form reserved.

(19–21). The Au/TiO_2 system is thus of great interest to both the catalyst scientist and theoreticians studying the electronic behavior of quantum size devices.

Three different Au/TiO_2 systems were studied, with size distributions varying between 1 and 10 nm. Emphasis was placed on attempting to resolve the crystal structure of the supported gold particles, to determine if the changes in activity observed between the three systems are related to changes in crystal structure.

2. EXPERIMENTAL

Interestingly, while the activity of Pt supported on TiO_2 is found to be almost independent of the preparation method used, the activity of Au/TiO_2 varies dramatically. Au/TiO_2 prepared by deposition–precipitation is normally active at temperatures well below 0°C and has activity much higher than that of Pt, but on the other hand, catalysts prepared by photodeposition are largely inert and show only marginal CO oxidation activity (22).

Catalysts with between 1.3 and 3.6 wt% loadings were prepared by three methods: deposition–precipitation in the presence of magnesium citrate (23), photodeposition (22), and normal deposition–precipitation followed by vacuum calcination (24). These catalysts are defined in subsequent text as Mg-cit Au/TiO_2, PD-Au/TiO_2, and vac-Au/TiO_2. For Au prepared by deposition–precipitation in the presence of magnesium citrate, the TiO_2 support used was JRC-TIO_4 (Degussa, surface area 50 m^2/g). For this experiment sufficient gold was present in the solution to give a theoretical maximum gold loading of 8 wt%. However, as is usual in deposition–precipitation preparations, a percentage of the gold fails to interact with the support and the final gold loading was determined to be only 3.0 wt% (chemical analysis carried out independently by Sumika Chemical Analysis Service, Ehime, Japan). From XRD measurements the support is mainly anatase with trace amounts of srilankite. The $HAuCl_4 \cdot 4H_2O$ used for deposition was of reagent grade and 99.5% purity, obtained from Kishida Chemicals Company. The major metal impurities in the chloroauric acid were Pt, Ir, and Pd, at 2, 7, and 11 ppm. However, the concentrations of trace elements within the Au/TiO_2 catalyst were below analytical detection levels, and the deposited gold, especially in the very small, nanometer particles, is considered pure. It may be noted that by simple calculations we can determine that for an average size of 1 to 5 nm (assuming 100 atoms per cluster) only about one Au cluster in every hundred should contain a Pt, Ir, or Pd impurity. This number is an upper limit and should decrease when the facts that (a) impurities generally concentrate only at defects and (b) recrystallization is by default a purification process are taken into account. Thus, as in all previous papers, it is considered unlikely that the presence of Pt or Pd impurities affects the activity of the system.

For the preparation of PD-Au/TiO_2 catalyst (22), 100 mg of TiO_2 was suspended in 4 ml of distilled water and agitated in an ultrasonic bath for 1 h. After agitation the TiO_2 was transferred to a quartz cell photoreactor. To the slurry a 1 : 1 (v/v) solution of water : methanol and $HAuCl_4$ sufficient to provide a 3.6 wt% loading was added. The pH of the suspension was then adjusted to 7, and the mixture deaerated with pure Ar (80 ml/min) for 30 min. After deaeration the suspension was irradiated with a high-pressure Hg lamp operated at 25 mW cm^{-2} at 313 K for 30 min. After irradiation the sample was washed in hot aqueous water to remove chlorine and vacuum-dried. The catalyst was then used without further treatment. Samples prepared by vacuum calcination followed the standard deposition–precipitation technique, outlined in Ref. (24). After the TiO_2 support was mixed in an aqueous solution of $HAuCl_4$ ($T_{soln} = 70$°C, pH 7.0) for 1 h, the catalyst was washed and the powder collected by filtration. The catalyst was then dried under vacuum and, without reexposure to air, calcined at 400°C for 4 h. The total gold loading deposited on vacuum-calcined Au/TiO_2 (vac-TiO_2) was 1.3 wt%. In all three preparations, for Debye function analysis (DFA), blank TiO_2 supports were also prepared with HCl used in place of the chloroauric acid.

Test for catalytic activity were carried out using 1% CO gas balanced in air with a space velocity of 20,000 ml h^{-1}/g cat. The reactor was a fixed-bed type, identical in design to that described in Ref. (25). As with previous publications the effect of moisture has not been included in the measurement of catalytic activities. Although, moisture levels strongly affect turnover frequencies (25), in these studies as we have operated all three catalysts under equivalent conditions of approximately similar water content, it was considered that the results were internally consistent and that no further studies were required.

For DFA experiments translucent pellets $8 \times 15 \times 0.2$ mm^3 in volume ($\mu d \approx 1.0$), of both the Au/TiO_2 catalysts and the TiO_2 support, were made by pressing the powder to a pressure of 4 tons/cm^2. Samples were then mounted in a specially designed reaction cell (26), which in turn was mounted on a commercial Guinier diffractometer (Huber). The cell was aligned 45° to the transmission geometry. To aid background subtraction of the support, diffraction patterns of both the Au/TiO_2 catalyst and TiO_2 support were taken simultaneously. X-rays of Cu$K\alpha_1$ wavelength were generated by a conventional X-ray source, with the energy defined using a Johansson-type Ge monochromator. An Al filter of 15-μm thickness mounted at the receiving slit was used to suppress Ti fluorescence.

After recording diffraction spectra for the Au/TiO_2 catalyst and the JRC-TIO_4 support, DFA of the difference spectra was carried out using three-dimensional model gold clusters created with and without crystal defect twin planes. From the atomic coordinates one can then calculate the

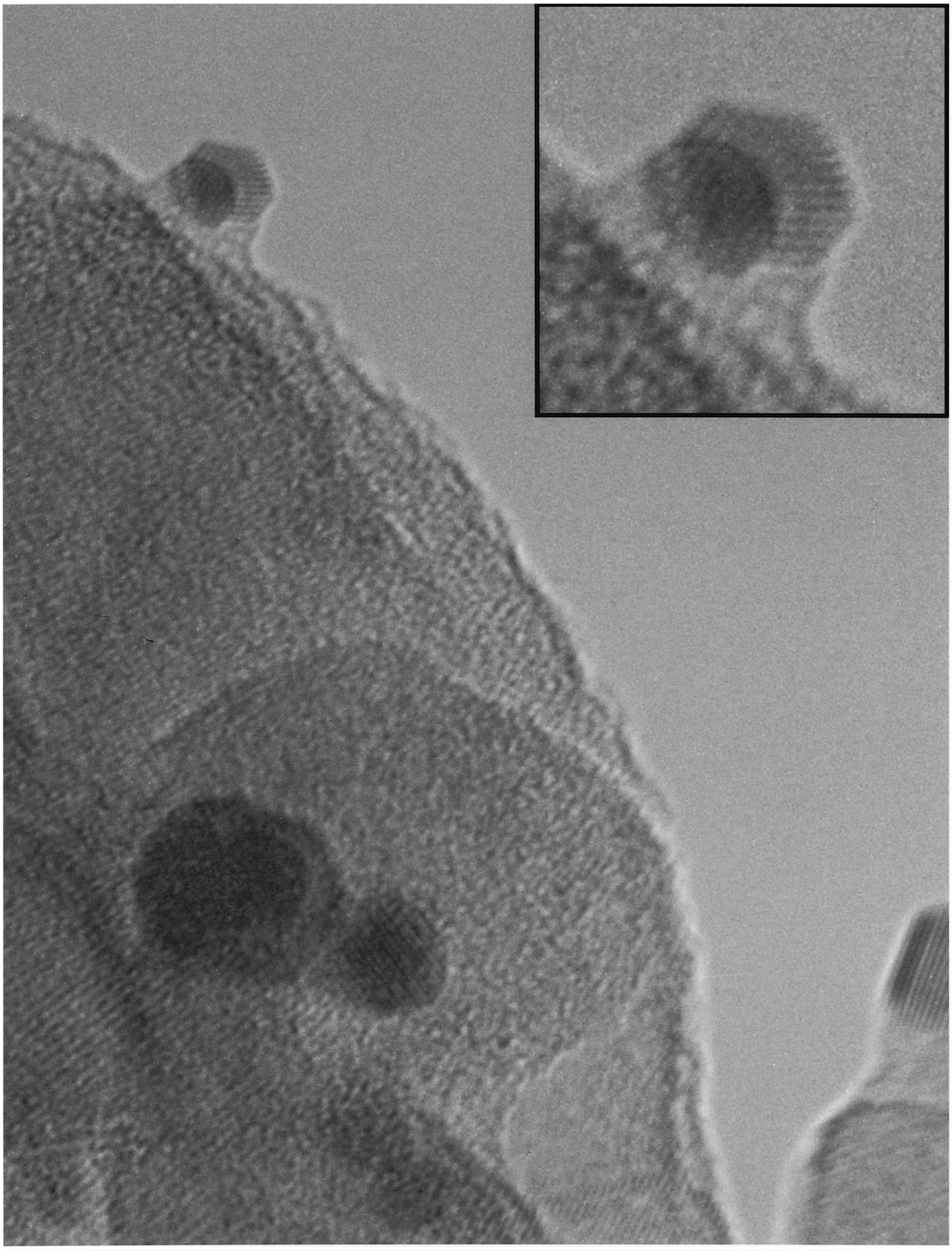

FIG. 1. High-resolution transmission electron micrograph of the 3 wt% Mg-cit Au/TiO_2 catalyst, revealing the presence of twinned gold particles and particles of semispherical shape. Inset: Highly amorphous region between the support and gold particle that suggests strong local reconstruction of the TiO_2 under the gold particle.

scattering intensity. The DFA is thus based largely on the summation of the scattering vector components from model clusters of incremental increasing size (27–33),

$$I_N = \sum_{n,m=1}^{N} f_n f_m[\sin(2\pi b r_{nm})]/(2\pi b r_{nm}),$$

where I_N is the total intensity and f is the scattering factor for species n and m. The term b refers to the scattering vector. For analysis, the summation is then directly compared with the experimental difference spectra, allowing both the size distribution and crystal symmetry to be extracted. Free parameters are used for calculating the number fractions of the individual clusters, with additional parameters used to define the exponent of the Debye–Waller factor, the mean interatomic distance averaged over all clusters, and to account for errors in the background subtraction. The quality of the fit is controlled by the R factor:

$$R = \left\{ \sum (I_{\text{obs}} - I_{\text{calc}})^2 \right\}^{1/2} \Big/ \sum I_{\text{obs}}.$$

Although particles of any size can be used, in practice analysis is carried out using magic numbers, with the particle size averaged using discrete closed-shell structures of gradually increasing size. This simplification in size distribution has been found to substantially ease data analysis, without deviating too much from the true continuous size distribution. Details of the method are given in Refs. (28, 29). Total surface exposures are calculated from DFA data by counting the number of surface atoms (N_s) of the model clusters used in the theoretical simulations. The total dispersion is the weight-averaged dispersion (N_s/N) of the individual model clusters (28). No assumption during this part of the analysis is made for blocking part of the surface by bonding to the support. It should also be noted that though the Debye functions of a fcc cuboctahedral array differ substantially between crystals of icosahedral and decahedral symmetry, as the Debye functions for two fcc crystals are nearly identical (even if they are of different particle shape) we are not usually able to distinguish between three-dimensional crystals that exist in the form of a sphere or a raft.

High-resolution transmission electron micrographs were recorded using a Hitachi H-9000 transmission electron microscope (TEM). All size distributions based on transmission electron micrographs were calculated by a manual search of approximately 200 particles, taken over 5 to 10 separate micrographs. Particle dimensions were determined automatically with the aid of a computerized image analyzer (Excel, Nippon Avionics Co. Ltd).

3. RESULTS

Transmission electron micrographs of 3 wt% Mg-cit Au/TiO_2 (Fig. 1) reveal two different morphologies for the gold particles: well-defined crystalline particles in which several faces can be clearly seen, and simple more spherical-type clusters. On a number of occasions twinning of the gold particles is clearly evident. Unfortunately the study of twins by TEM is extremely difficult due to the need to align the particle with a high degree of precision perpendicular to the electron beam, and the absolute percentage of particles present that contain twins is largely uncertain. Where twins are seen in the transmission electron micrographs, most occur in the larger particles, suggesting perhaps that the twinned particles form by the coalescence of two or more smaller particles. This result is in agreement with previous TEM studies which show that most large polycrystalline structures appear to comprise multiple twinned particles that rapidly fragment or rearrange under study (34). Between the gold and TiO_2 support the structure of the support is highly amorphous.

The TEM-related size distribution shown in Fig. 2 tends to be inhomogeneous for PD-Au/TiO_2, extending from 1 to 14 nm in size (22). Again, the shape of the crystal (not shown) tends to be largely irregular, varying with the size of the crystal. Analysis of the 1.3 wt% vac-Au/TiO_2 catalyst was complicated by the apparent low concentration of gold in the metallic state. Normally, during vacuum calcination, the gold precursor remains an ionic species, which coalesces to the Au metal only slowly under oxidative reaction conditions (24). On exposure to a TEM electron beam, however, the particles rapidly coalesced to between 1 and

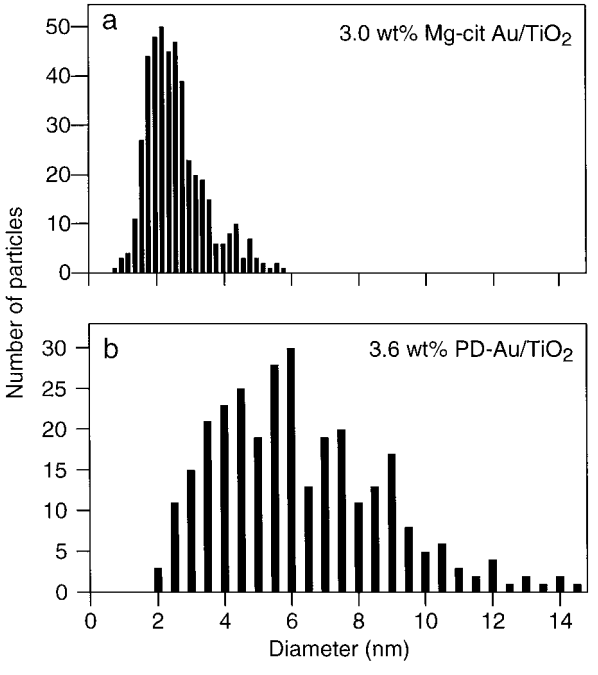

FIG. 2. TEM-calculated size distributions of the deposited Au particles present in (a) 3 wt% Mg-cit Au/TiO_2 and (b) 3.6 wt% PD-Au/TiO_2 (22). In photodeposited gold the size distribution extends to 14 nm.

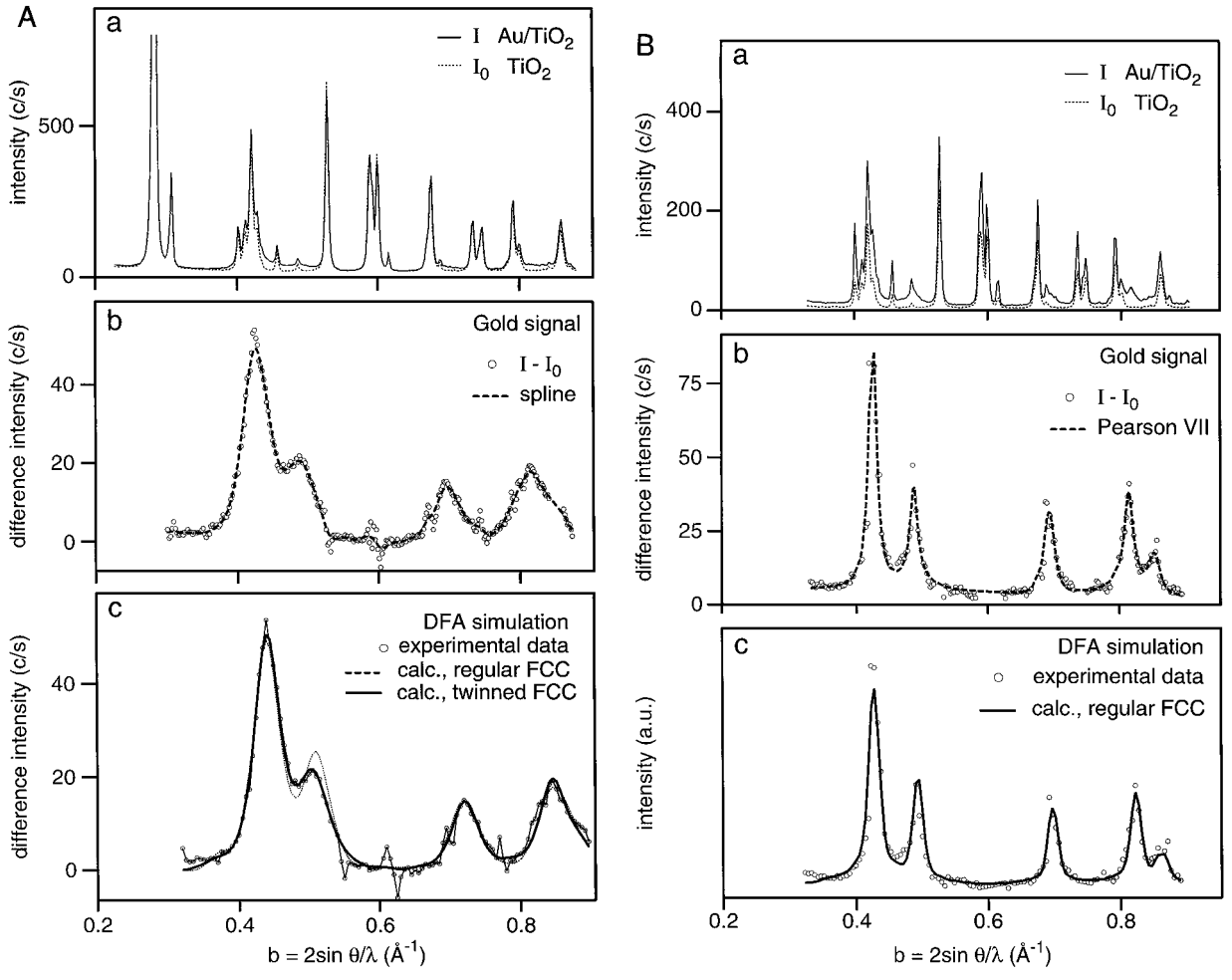

FIG. 3. (A) X-ray diffraction patterns for (a) 3 wt% Mg-cit Au/TiO_2 (solid line) and the TiO_2 support (dashed line), (b) the X-ray difference intensity, and (c) Debye function analysis assuming the presence of (dotted line) only single fcc cuboctahedral gold particles and (solid line) single twinned fcc gold particles. In the latter case the *R* factor improves from 2.2 to 1.6%. (B) X-ray diffraction patterns for (a) 3.6 wt% PD-Au/TiO_2 (solid line) and the TiO_2 support (dashed line), (b) the X-ray difference intensity, and (c) Debye function analysis assuming fcc cuboctahedral gold. The *R* factor is 2.7% for this simulation.

2 nm in size. As a result, the original shape and size distribution of the gold particles in vac-Au/TiO_2 could not be determined.

DFA (Figs. 3A and 4) of 3 wt% Mg-cit Au/TiO_2, taken 1 week after preparation, reveals the average size of the gold particles present to be on the order of 3.0 ± 0.3 nm, with 42 ± 5% of the gold atoms located at the surface. Figure 3A shows (a) the original intensity of the Au/TiO_2 catalyst taken 1 week after preparation and the TiO_2 support, (b) the difference signal, and (c) the simulation of the experimental difference spectra by Debye functions. In part (c) of the analysis the experimental data are converted so that they are equidistant along the *b* scale, resulting in the slight change in the appearance of the data. No change in size distribution or crystal structure was observed either during or after catalytic studies, indicating that for 3 wt% Mg-cit Au/TiO_2, the Au is structurally stable during CO oxidation. On average the calculated size distributions obtained for each catalyst by DFA (Fig. 4) agreed closely with those obtained by TEM.

In Fig. 3A it can be seen that though the general fit for the 3 wt% Mg-cit Au/TiO_2 catalyst is reasonable, in the vicinity of the 200 peak, at approximately $b = 0.48$ Å^{-1}, a slight difference does occur. According to Warren, the 200 peak is the most sensitive to the presence of twinning and/or deformation faults (35). Theoretically these stacking faults should broaden and slightly shift the 200 peak inward, as seen with the actual experimental data for 3 wt% Mg-cit Au/TiO_2. The presence of twins would also agree with the work of Patil *et al.* (15) who has previously stated that multiple twinned particles are theoretically the most stable crystallographic structure at nanometer sizes. Cleveland *et al.* (16, 17) have also stated the same and that although the Marks decahedra is classified as being a multiple twinned

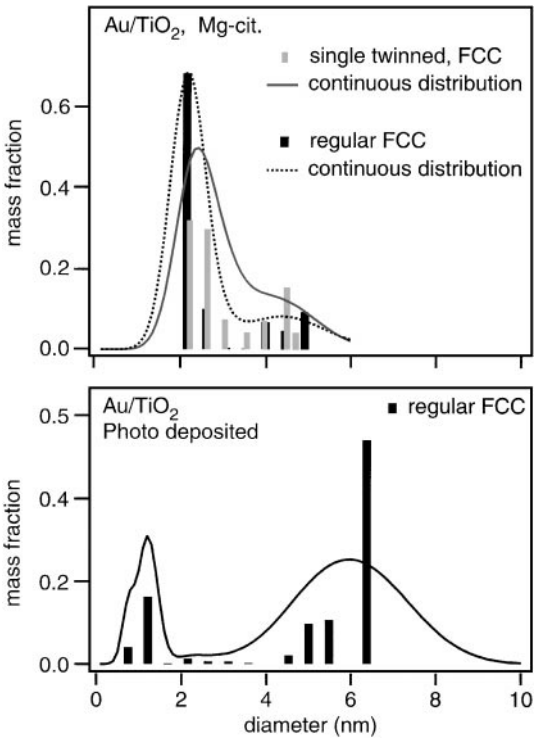

FIG. 4. DFA-calculated size distribution of the gold particles present in (a) 3 wt% Mg-cit Au/TiO_2 and (b) 3.6 wt% PD-Au/TiO_2. The discrete bars correspond to the sphere-equivalent cluster diameters. The solid lines represent a continuous size distribution that fits equally well to the experiment (28). The latter are calculated by convolution of the discrete size distributions with Gaussians of constant relative width $\Delta D/D$, where ΔD is the diameter increment of the model clusters. For Mg-cit Au/TiO_2 the result of the two simulations (compare Fig. 3A) are plotted in the top graph. The difference between these two distributions relates to the errors of the DFA method.

structure, for this specific decahedra intrinsic strains are substantially reduced.

On accounting for the presence of crystallographic twins in the DFA analysis (Fig. 3A, c) an improvement in the quality of the 3 wt% Mg-cit Au/TiO_2 spectrum was observed using model clusters that contain one single twin (solid line). Due to limits in computing time and the almost infinite number of permutations possible (e.g., ensembles of nontwinned and multiply twinned particles) only single twinning was considered in the calculation. To quantify the degree of twinning, we use the usual bulk parameter β for the twin probability ($\beta =$ number of twin planes divided by total number of net planes parallel to the twin plane). For small particles the average number of 111 planes per particle is D_N/d_{111}, which equals 11 (2.5/0.23) ($D_N =$ number average of diameters, $d_{111} =$ (111) netplane distance). Thus the twin probability β can be estimated to be 1/11, or 9%.

In contrast to the 3 wt% Mg-cit Au/TiO_2 catalyst, the 3.6 wt% PD-Au/TiO_2 catalyst (Fig. 3B) clearly exhibits a narrow X-ray diffraction peak overlying a broad underlying wing that slowly changes in intensity. This structure qualitatively indicates a broad size distribution going from small to large sizes.

In Fig. 4b an optimized DFA fit for 3.6 wt% PD-Au/TiO_2 gives a mass mean diameter of approximately 6 nm, with about 20% percent of the gold existing in the form of 0.7- to 1.2-nm particles, containing ~55 or fewer atoms. This implies that 33% of the contained gold is located at the surface. From a DFA the larger crystals also appear to be of fcc symmetry, indicating that irrespective of the deposition method, the cuboctahedral symmetry forms at between 2 and 8 nm. A slight broadening of the high-order peaks is also observed which on fitting the line profiles by Pearson VII functions indicates an internal microstrain $\varepsilon_{111} \sim 0.6\%$ along the [111] direction, presumably originating from grain boundaries within the larger crystals. From the calculation of the integral linewidth shown in Fig. 5 one can also measure a mass average gold particle diameter of 7.0 ± 1 nm for the PD-Au/TiO_2 sample, which is comparable in value to that given by DFA. The contribution of stacking faults to the linewidth is below the detection limit.

DFA of the 1.3 wt% vac-TiO_2 catalyst (Fig. 6) was restricted by the low concentration of gold that exists in the metallic state. This results in an extremely weak difference spectrum, lying at the limits of detection. From a preliminary analysis, however, it is possible to determine that the particle size of the gold is between 1 and 2 nm and the structure is, again, mainly fcc cuboctahedral. As mentioned before, in the vacuum-calcined TiO_2 system most of the gold is apparently in the ionic state (24) and thus not analyzable by the DFA technique. For these reasons and also because

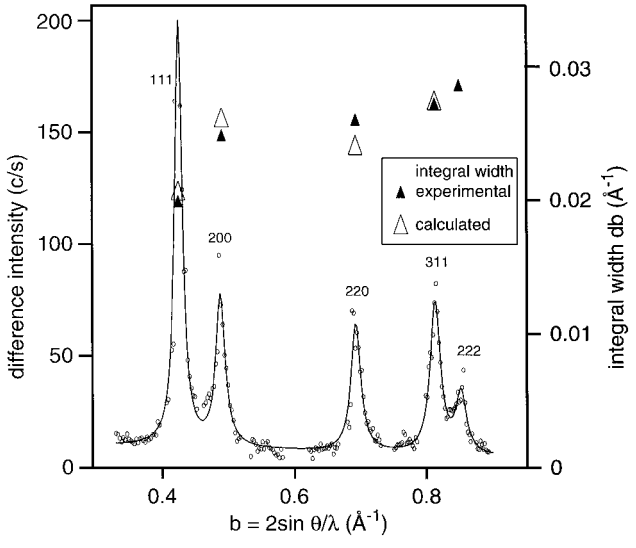

FIG. 5. Difference intensity for 3.6 wt% PD-Au/TiO_2 (circles) and peak fitting with Lorentzian-type Pearson VII functions (solid line). The integral linewidths deduced from the fit are displayed on the right axis (filled triangles). According to Warren (35) linewidth can be fitted by using mass mean crystallite size, internal microstrains, and stacking faults as free parameters (open triangles).

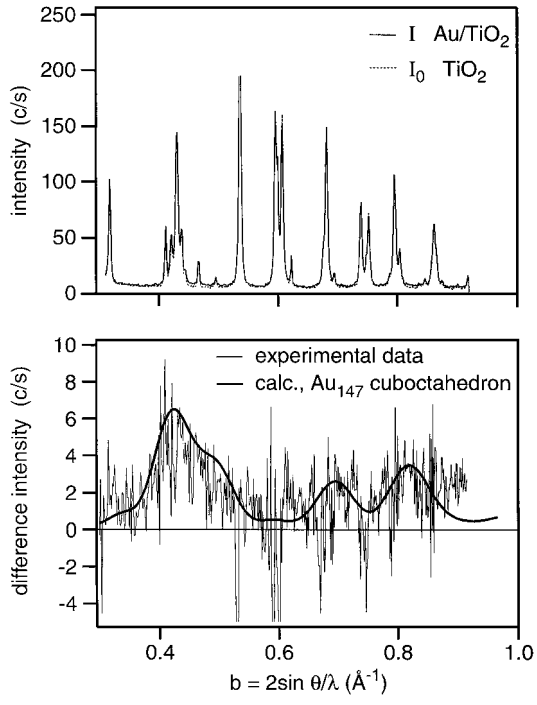

FIG. 6. XRD patterns of Au/TiO_2 and TiO_2 calcined under vacuum. The difference signal shown in the lower panel is very weak and cannot be used for DFA. A crude value for the gold cluster size of this catalyst is obtained by comparison with single Debye functions. A fcc-type three-shell cuboctahedron Au_{147} ($D = 1.7$ nm) fits best to the difference pattern (solid line).

atomic absorption provides only the total gold content and not the total content of gold in the metal state, it was not possible to determine the turnover frequency for this catalyst (Table 1).

4. DISCUSSION AND CONCLUSIONS

In making conclusions based on the given results it is worthwhile to bear a number of points in mind. In catalysis quite often very little is known concerning the behavior of Au particles or, indeed, any other ultrasmall materials. Transmission electron microscopy and other related techniques (36) have in recent years been used, but are often limited by two problems: first they analyze only a limited area of the catalyst and second they require the catalyst to be studied under conditions far from those we actually use in tests. The alternative X-ray technique, EXAFS, which has gained widespread use in recent years, though beneficial in many respects, is surprisingly of limited use in studying nanoparticles. This is probably due to the need in EXAFS for the sample to be homogeneous, so that data analysis can be simplified, and also because of the complex overlap of four competing signals caused by atoms located at (i) the interface between the gold particle and the support; (ii) the periphery between the gold, the support, and air molecules; (iii) the surface gold atoms exposed only to the air phase, and (iv) the bulk Au atoms located at the center of the particle. The EXAFS technique is therefore incapable of determining the crystal symmetry of the Au particle and was therefore not used in this study.

TABLE 1

Calculated Size Distributions and Turnover Frequencies for Vac-Au/TiO_2, Mg-cit Au/TiO_2, and PD-Au/TiO_2 Catalyst[a]

Sample	Size range (nm)	Crystal type	$T_{1/2}$	Surface exposed	TOF (203 K)	Twin probability
1.3% vac.	1–2	fcc	298 K	NA[b]	NA[a]	NA
3% Mg-cit	2–3	fcc	203 K	44%	3.7×10^{-2}	9%
3.6% PD	1–8	fcc	>523 K	33%	5×10^{-7}	<1%

[a] The TOF for vacuum-calcined catalyst could not be determined due to insufficient information on the fraction of gold present in the metallic form.

[b] Not analyzed.

In previous work (6, 7) for Au supported on $Mg(OH)_2$, the main active species is gold in the icosahedral symmetry. This conclusion is based on observations that higher catalytic activity occurs only with increasing icosahedral content in the catalyst and also agrees with the observation that high activities are seen in $Au/Mg(OH)_2$ catalyst only when the particle is smaller than 1 nm, or in other words in the size region where theoretically the icosahedral particles first become stable.

The results obtained here, for the Au/TiO_2 system, thus differ from those for $Au/Mg(OH)_2$ catalyst in the crystal structure which is active. In all three Au/TiO_2 catalysts the active crystal structure is of fcc symmetry. We are therefore forced to consider that either (a) a different reaction route is involved in the case of TiO_2, which would imply that the reaction does not take place on the gold (this is considered unlikely based on our previous knowledge that TiO_2 is inactive), or (b) the reaction takes place at the interface between gold and the support, in other words, the catalytic activity is related to the structure of both the gold and support species.

Due to the different crystal symmetries between the previously studied $Au/Mg(OH)_2$ system (6, 7) and the Au/TiO_2 system, which we studied in this paper, it is therefore probable that each gold catalyst must now be considered separately (4). The ability of Au/TiO_2 to catalyze CO oxidation using fcc cuboctahedral symmetry gold particles, whereas for $Au/Mg(OH)_2$ the icosahedral structure is required, directly implies that the reaction must take place at the interface and that the structures of both the gold particle and the underlying (amorphous) support are important in determining the overall activity. From our studies of gold catalysts over many years this appears entirely reasonable. Gold is able to induce a low-temperature oxidation reaction over

alkaline earths, transition metal elements, and also p-block species such as SiO_2 (37–41), despite the large differences in electronic properties that exist between them. It is therefore apparent that with changes in the structure of Au and the support, gold-based catalysts are highly complex. Clearly, further work is required to determine the structure of the interface and also to determine whether defects such as twinning planes affect the overall activity.

ACKNOWLEDGMENT

The authors acknowledge, during this work and on many other occasions, the kind assistance given by Ms. T. Nakamura in calculating the size distributions by TEM.

REFERENCES

1. Pireaux, J. J., Chtaib, M., Delrue, J. P., Thiry, P. A., Liehr, M., and Caudano, R., *Surf. Sci.* **141**, 211, 221 (1984).
2. Evans, S., Evans, E. L., Parry, D. E., Tricker, M. J., Walters, M. J., and Thomas, J. M., *Chem. Soc. Faraday Discuss.* **58**, 1975 (1975).
3. Lazaga, M. A., Wickham, D. T., Parker, D. H., Kastanas, G. N., and Koel, B. E., *in* "Catalytic Selective Oxidation" (S. T. Ooyama and J. W. Hightower, Eds.), ACS Symp. Ser. 523, pp. 90–109. Am. Chem. Soc., Washington, DC, 1993.
4. Bollinger, M. A., and Vannice, M. A., *Appl. Catal. B* **8**, 417 (1996).
5. Outka, D. A., and Madix, R. J., *J. Am. Chem. Soc.* **109**, 1708 (1987).
6. Vogel, W., Cunningham, D. A. H., Tanaka, K., and Haruta, M., *Catal. Lett.* **40**, 175 (1996).
7. Cunningham, D. A. H., Vogel, W., Kageyama, H., Tsubota, S., and Haruta, M., *J. Catal.* **177**, 1 (1998).
8. Mackay, A. L., *Acta Crystallogr.* **15**, 916 (1962).
9. Uppenbrink, J., and Wales, D. J., *J. Chem. Phys.* **96**, 8520 (1992).
10. Buffat, P. A., Flüeli, M., Spycher, R., Stadelmann, P., and Borel, J. P., *Faraday Discuss.* **92**, 173 (1991).
11. Sawada, S., and Sugano, S., *NATO ASI Ser. Serc.* **1**, 119 (1992).
12. Sawada, S., and Sugano, S., *in* "Physics and Chemistry of Finite Systems: From Clusters to Crystals" (P. Jena, S. N. Khanna, and B. K. Rao, Eds.), Vol. 1, p. 119. Kluwer, Dordrecht, 1992.
13. Kumar, J., and Gupta, A., *in* "Physics and Chemistry of Finite Systems: From Clusters to Crystals" (P. Jena, S. N. Khanna, and B. K. Rao, Eds.), Vol. 1, p. 93. Kluwer, Dordrecht, 1992.
14. D'Agostino, G., Pinto, A., and Mobilio, S., *Phys. Rev. B* **48**, 14447 (1993).
15. Patil, A. N., Paithankar, D. Y., Otsuka, N., and Andres, R. P., *Z. Phys. D* **26**, 135 (1983).
16. Cleveland, C. L., Landman, U., Shafigullin, M., Stephens, P. W., and Whetten, R. L., *Z. Phys. D* **40**, 503 (1997).
17. Cleveland, C. L., and Landman, U., *J. Chem. Phys.* **94**, 7376 (1991).
18. Whetten, R. L., Khoury, J. T., Alvarez, M. M., Murphy, S., Vezmar, I., Wang, Z. L., Stephens, P. W., Cleveland, C. L., Luedtke, W. D., and Landman, U., *Adv. Mater.*, 428 (1996).
19. Han, L., Tsubota, S., Kobayashi, T., and Haruta, *J. Chem. Soc. Chem. Commun.*, 93 (1995).
20. Hayashi, T., Tusbota, S., and Haruta, M., *Ind. Eng. Chem. Res.* **34**, 2298 (1995).
21. Tanaka, K., Hayashi, T., and Haruta, M., *J. Jpn. Inst. Metals* **60**, 693 (1996).
22. Bamwenda, G. R., Tsubota, S., Nakamura, T., and Haruta, M., *Catal. Lett.* **44**, 83 (1997).
23. Torres Sanchez, R. M., and Haruta, M., *in* "Proceedings, XVth Iberoamerican Symposium on Catalysts, Cordoba, June 1996."
24. Cunningham, D. A. H., Tsubota, S., Kamijo, N., and Haruta, M., *Res. Chem. Intermediates* **19**, 1 (1993).
25. Cunningham, D. A. H., Kobayashi, T., Kamijo, N., and Haruta, M., *Catal. Lett.* **25**, 257 (1994).
26. Hartmann, N., Imbihl, R., and Vogel, W., *Catal. Lett.* **28**, 373 (1994).
27. Debye, P., *Ann. Phys.* **46**, 807 (1915).
28. Gnutzmann, V., and Vogel, W., *J. Phys. Chem.* **94**, 4991 (1990).
29. Vogel, W., Rosner, B., and Tesche, B., *J. Phys. Chem.* **97**, 11611 (1993).
30. Vogel, W., and Sachtler, W. M. H., *Z. Zhang Ber. Bunsenges. Phys. Chem.* **97**, 280 (1993).
31. Vogel, W., and Duff, D. G., *Langmuir* **11**, 401 (1995).
32. Kazakov, A. V., Shapiro, E. S., and Voskoboinikov, T. V., *J. Phys. Chem.* **99**, 8323 (1995).
33. Hall, B. D., Flueli, R., Monot, R., and Borel, J. P., *Z. Phys. D At. Mol. Clusters* **12**, 97 (1989).
34. Iijima, S., and Ichihashi, T., *Phys. Rev. Lett.* **56**, 616 (1986).
35. Warren, B. E., "X-ray Diffraction," pp. 253, 303. Addison-Wesley, Reading, MA.
36. Haruta, M., Yamada, N., Kobayashi, T., and Iijima, S., *J. Catal.* **115**, 301 (1989).
37. Li, Y. Z., Reifenberger, R., Choi, E., and Andre, R. P., *Surf. Sci.* **250**, 1 (1991).
38. Haruta, M., Tsubota, S., Kobayashi, T., Kageyama, H., Genet, M. J., and Delmon, B., *J. Catal.* **144**, 175 (1993).
39. Haruta, M., *Catal. Today* **36**, 153 (1997).
40. Tsubota, S., Cunningham, D. A. H., Bando, Y., and Haruta, M., *in* "Preparation of Heterogeneous Catalysts" (G. Poncelet *et al.*, Eds.), p. 227. (1995).
41. Haruta, M., Kobayashi, T., Tsubota, S., and Nakahara, Y., *Chem Express* **3**, 159 (1988).